JCTC Journal of Chemical Theory and Computation

Article

pubs.acs.org/JCTC

Direct-Space Corrections Enable Fast and Accurate Lorentz−Berthelot Combination Rule Lennard-Jones Lattice Summation

Christian L. Wennberg, Teemu Murtola, Szilárd Páll, Mark J. Abraham, Berk Hess, and Erik Lindahl*

Swedish e-Science Research Center, Department of Theoretical Physics, KTH Royal Institute of Technology, Box 1031, 171 21 Solna, Sweden

Center for Biomembrane Research, Department of Biophysics & Biochemistry, Stockholm University, 106 91 Stockholm, Sweden

ABSTRACT: Long-range lattice summation techniques such as the particle-mesh Ewald (PME) algorithm for electrostatics have been revolutionary to the precision and accuracy of molecular simulations in general. Despite the performance penalty associated with lattice summation electrostatics, few biomolecular simulations today are performed without it. There are increasingly strong arguments for moving in the same direction for Lennard-Jones (LJ) interactions, and by using geometric approximations of the combination rules in reciprocal space, we have been able to make a very high-performance implementation available in GROMACS. Here, we present a new way to correct for these approximations to achieve *exact* treatment of Lorentz−Berthelot combination rules within the cutoff, and only a very small approximation error remains outside the cutoff (a part that would be completely ignored without LJ-PME). This not only improves accuracy by almost an order of magnitude but also achieves absolute biomolecular simulation performance that is an order of magnitude faster than any other available lattice summation technique for LJ interactions. The implementation includes both CPU and GPU acceleration, and its combination with improved scaling LJ-PME simulations now provides performance close to the truncated potential methods in GROMACS but with much higher accuracy.

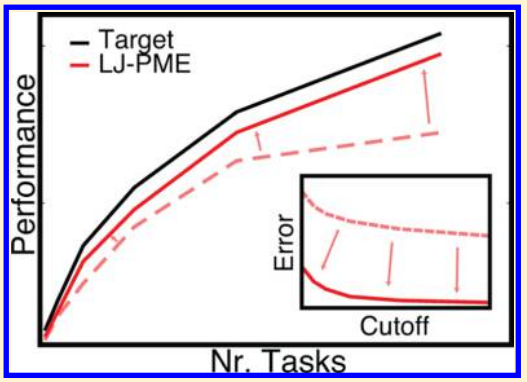

1. INTRODUCTION

The particle-mesh Ewald (PME) algorithm developed by Darden and co-workers[1,2] has been the method of choice for long-range electrostatic interactions in molecular dynamics (MD) simulations of biological systems for the past decade. Previously, these interactions were treated with cutoffs after a fixed distance, which has been shown to yield severe artifacts in calculated properties.[3−8] While these artifacts were avoided with PME, the initial implementations were computationally expensive (typically 2−3× times slower), and it was first with the improved smooth PME[2] and later with accelerated implementations by several groups (see, e.g., ref 9) that the performance improved to the point where PME electrostatics became the defacto standard in biomolecular simulations. In their early papers, Darden et al. already noted how the PME method could be extended to include any interaction for which the potential decayed as $r^{-\alpha}$ (assuming $\alpha \geq 1$), and one such obvious extension of the method would be to apply it to calculate the dispersive component of Lennard-Jones (LJ) interactions. However, the implementation of Lennard-Jones PME (LJ-PME) turned out to be extremely challenging since the Lorentz−Berthelot (LB) combination rules used to derive the interaction coefficients for mixed particle types in many force fields required six separate Fourier transforms. This led to a gigantic performance penalty that was much larger than that for electrostatics PME. Since the LJ truncation errors are both smaller than electrostatics one and since it is possible to apply analytical dispersion corrections, LJ-PME never caught on. Given the increasing accuracy requirements for sensitive, heterogeneous, and anisotropic systems such as membranes, we argue that it is time to change this practice, and we believe this study introduces an LJ-PME implementation that provides both the performance and accuracy to replace analytical dispersion corrections.

Currently, most simulations of biologically relevant systems utilize cutoffs in the range of 10−14 Å for LJ interactions. In particular, for systems like lipid bilayers that are highly sensitive to dispersion effects, it is common to employ longer cutoffs and also to correct for the missing energy through an analytical dispersion correction

$$U_{\mathrm{dc}} = \frac{N}{2}\rho \int_{r_c}^{\infty} 4\varepsilon\left[\left(\frac{\sigma}{r}\right)^{12} - \left(\frac{\sigma}{r}\right)^{6}\right] g(r)\, 4\pi r^2\, \mathrm{d}r \qquad (1)$$

Here, N is the number of particles in the system, ρ is their average number density, and σ and ε are the interaction coefficients that are approximated as average parameters. $g(r)$ is the pair distribution function that is approximated with unity outside the cutoff, which enables us to evaluate the integral as

Received: July 30, 2015
Published: November 4, 2015

DOI: 10.1021/acs.jctc.5b00726
J. Chem. Theory Comput. 2015, 11, 5737−5746

$$U_{dc} = 8N\pi\rho\varepsilon\sigma^3\left[\frac{1}{9}\left(\frac{\sigma}{r_c}\right)^9 - \frac{1}{3}\left(\frac{\sigma}{r_c}\right)^3\right] \quad (2)$$

However, the use of this correction term in simulations of different types of interfaces (e.g., lipid bilayers) is troublesome since the assumption that $g(r)$ is equal to unity beyond the cutoff inherently assumes that the system is homogeneous and isotropic, something that most definitely is not true for these systems. The implication of this for simulations containing lipid bilayers has not received much attention in the past, but when it is coupled to the development of alternative ways of treating long-range LJ interactions,[10−17] the problem has started to become more apparent over the past few years. In light of this, the first mesh-based dispersion solver, based on the particle−particle particle-mesh Ewald method,[18] was recently implemented in the LAMMPS[19] molecular dynamics package through the work of Isele-Holder et al.[20,21] Furthermore, we recently presented an implementation in the GROMACS simulation package where the PME method was used to calculate long-range LJ interactions.[22] In this implementation, we proposed circumventing the expensive calculations for the reciprocal sum by approximating the reciprocal-space interaction coefficients with the geometric combination rules[23] even where the force field uses LB rules.[24] While this introduced slight errors in the entire reciprocal space component (which extends inside the cutoff, too), we argued that this was at least smaller than the errors historically accepted with analytical dispersion corrections.

Here, we present a new idea to correct for these approximations, where we modify the evaulation of the direct-space potential in order to correct for the errors introduced with the approximated combination rules in reciprocal space. This direct-space modification *completely* cancels all approximation errors in the reciprocal space combination rules inside the cutoff, which means that the resulting total interaction is exact even for LB combination rules up to the cutoff (both direct and recpirocal space components). While there is still a small approximation error remaining outside the cutoff, this should be compared to the practice of completely ignoring all effects outside the cutoff or merely using the analytical correction based on average parameters. Furthermore, we have improved the performance and scaling of LJ-PME so that it now is comparable to GROMACS simulations using cutoffs with dispersion corrections to handle long-range LJ interactions. To the best of our knowledge, this is about an order of magnitude faster than any other available implementation.

2. THEORY

2.1. Lattice Summation of Dispersion Interactions. Given N particles at positions $\mathbf{r}_1$, $\mathbf{r}_2$, ..., $\mathbf{r}_n$ within the unit cell U, we can describe a general $r^{-\alpha}$ interaction between them as

$$U_\alpha = \frac{1}{2}\sum_{\mathbf{n}}{}' \sum_j \sum_k \frac{C(j,k)}{|\mathbf{r}_{jk} + \mathbf{n}|^\alpha} \quad (3)$$

where the outer sum is over the lattice translation vectors $\mathbf{n}$, $C(j,k)$ is the combined interaction coefficient, $\mathbf{r}_{jk} = \mathbf{r}_j - \mathbf{r}_k$ is the interparticle distance, and $'$ indicates that terms with $j = k$ are omitted when $\mathbf{n} = 0$.

For interactions with $\alpha \leq 3$ (such as electrostatics), this sum does not converge if the system has a net charge. For neutral systems, it can be made conditionally convergent (i.e., if the terms are added in the right order), but even then the convergence is very slow. For this reason, a lot of work has been invested in further developing the general solution, derived by Ewald,[25] in order to be applicable to molecular simulations as well.[1,2,15,21,26−28]

Following the derivation of Essman,[2] the expression above, applied to dispersion interactions, can be rewritten as

$$U_{\text{dispersion}} = \frac{1}{2}\sum_{\mathbf{n}}{}' \sum_j \sum_k \frac{C(j,k)\, g(\beta|\mathbf{r}_{jk} + \mathbf{n}|)}{|\mathbf{r}_{jk} + \mathbf{n}|^6} + \frac{\pi^{3/2}\beta^3}{2\mathbf{V}} \sum_{\mathbf{m}} f(\pi|\mathbf{m}|/\beta) \times \sum_j \sum_k C(j,k) \exp[-2\pi i \mathbf{m}\cdot\mathbf{r}_{jk}] - \frac{\beta^6}{12}\sum_j C(j,j) \quad (4)$$

with $\mathbf{m}$ being the reciprocal lattice vectors and β, the Ewald splitting parameter. The first and second terms are the direct and reciprocal interaction potentials, respectively, and the third term constitutes the self-energy. The expressions for $f(\pi|\mathbf{m}|/\beta)$ and $g(\beta|\mathbf{r}_{jk} + \mathbf{n}|)$ are given by

$$f(x) = 1/3[(1 - 2x^2)\exp(-x^2) + 2x^3\sqrt{\pi}\ \text{erfc}(x)] \quad (5)$$

$$g(x) = \exp(-x^2)\left(1 + x^2 + \frac{x^4}{2}\right) \quad (6)$$

Assuming the interaction coefficients $C(j,k)$ can be factorized, $C(j,k) = \sqrt{C(j,j)}\cdot\sqrt{C(k,k)}$, we can remove the double sum in the second term of eq 4 by defining the so-called structure factors, $S(\mathbf{m})$, as

$$S(\mathbf{m}) = \sum_j^N C(j,j)\exp[2\pi i \mathbf{m}\cdot\mathbf{r}_j] \quad (7)$$

which translates this second term into

$$\frac{\pi^{3/2}\beta^3}{2\mathbf{V}}\sum_{\mathbf{m}} f(\pi|\mathbf{m}|/\beta) \times S(\mathbf{m})\, S(-\mathbf{m}) \quad (8)$$

on which we can apply the PME methodology in the same way as is done for electrostatic interactions. This makes it relatively painless to use LJ-PME together with force fields that utilize geometric combination rules ($C(j,k) = \sqrt{\sigma_j\sigma_k}$). However, if the force field combines the coefficients according to the LB rules, then the coefficient $C(j,k)$ instead splits into seven terms

$$C(j,k) = (\sigma_j + \sigma_k)^6 = \sum_{n=0}^{6} P_n \sigma_j^n \sigma_k^{(6-n)} \quad (9)$$

which thereby also forces the splitting of the reciprocal dispersion energy into seven terms

DOI: 10.1021/acs.jctc.5b00726
J. Chem. Theory Comput. 2015, 11, 5737−5746

$$S(\mathbf{m})\,S(-\mathbf{m}) = \sum_{j,k}\sum_{n=0}^{6} P_n \sigma_j^n \sigma_k^{(6-n)} \exp(2\pi i \mathbf{m}\cdot\mathbf{r}_{jk}) = \sum_{n=0}^{6} P_n \Big[\sum_j \sigma_j^n \exp(2\pi i \mathbf{m}\cdot\mathbf{r}_j)\Big]\Big[\sum_k \sigma_k^{(6-n)} \exp(-2\pi i \mathbf{m}\cdot\mathbf{r}_k)\Big] = \sum_{n=0}^{6} P_n Z_n(\mathbf{m})\, Z_{6-n}(-\mathbf{m}) \tag{10}$$

where $Z_\alpha(\mathbf{m}) = \sum_j \sigma_j^\alpha \exp(2\pi i \mathbf{m}\cdot\mathbf{r}_j)$ and P_n are the Pascal triangle coefficients.

This effectively makes the PME method impractical to use together with force fields utilizing LB combination rules since the reciprocal interactions require the evaluation of several separate fast Fourier transforms (FFTs). As we have shown previously,[22] it is possible to circumvent this problem by approximating the interaction coefficients in reciprocal space using geometric combination rules, and this should not cause any serious effects in normal production runs. However, the approximation still results in an error, and in some simulations that are highly sensitive to the total energy, it would be preferable to avoid it. In the following, we present a way to modify the direct-space interactions in order to reduce the introduced error to a level where it is completely negligible.

2.2. Correcting the Reciprocal Energy in Direct Space.

From eq 3, we can see that the dispersion energy in our system is calculated as

$$U_{\text{dispersion}} = \frac{1}{2}\sum_{\mathbf{n}}{}' \sum_j \sum_k \frac{C_6^{jk}}{|\mathbf{r}_{jk}+\mathbf{n}|^6} \tag{11}$$

with C_6^{jk} being the combined dispersion coefficient. Using Ewald summation, we split this slowly converging sum into two sums

$$U_{\text{dispersion}} = \underbrace{\frac{1}{2}\sum_{\mathbf{n},j,k} \frac{C_6^{jk}\, g(\beta|\mathbf{r}_{jk}+\mathbf{n}|)}{|\mathbf{r}_{jk}+\mathbf{n}|^6}}_{\text{sum in direct space}} + \underbrace{\frac{1}{2}\sum_{\mathbf{n},j,k} \frac{C_6^{jk,\text{recip}}[1-g(\beta|\mathbf{r}_{jk}+\mathbf{n}|)]}{|\mathbf{r}_{jk}+\mathbf{n}|^6}}_{\text{sum in reciprocal space}} \tag{12}$$

where the function $g(\beta|\mathbf{r}_{jk}+\mathbf{n}|)$ is given by eq 6, $C_6^{jk,\text{recip}}$ is the dispersion coefficient used for the reciprocal sum (i.e., not necessarily equal to the true C_6^{jk}), and we have defined $\sum_{\mathbf{n},j,k} = \sum_{\mathbf{n}}{}'\sum_j^N\sum_k^N$. The first sum in eq 12 is a fast converging sum in direct space, whereas the second sum is a slowly varying function of $|\mathbf{r}_{jk}+\mathbf{n}|$, thus making its Fourier transform a fast converging sum in reciprocal space.

For our first implementation and the case where $C_6^{jk,\text{recip}} \neq C_6^{jk}$, this gave the total interaction energy within the cutoff as

$$U_{\text{dispersion}} = \frac{1}{2}\sum_{\mathbf{n},j,k} \frac{C_6^{jk,\text{recip}}}{|\mathbf{r}_{jk}+\mathbf{n}|^6} + \frac{1}{2}\sum_{\mathbf{n},j,k} \frac{(C_6^{jk}-C_6^{jk,\text{recip}})\, g(\beta|\mathbf{r}_{jk}+\mathbf{n}|)}{|\mathbf{r}_{jk}+\mathbf{n}|^6} \tag{13}$$

which maintains a well-defined Hamiltonian while keeping the associated error at a negligible level (less than 0.5% of total dispersion energy) in the production runs that we performed.[22] Comparing these equations, it would be possible to achieve a more correct implementation of the original potential by also modifying the direct-space calculations so that we subtract the reciprocal contribution from the original dispersion potential in eq 11:

$$\begin{aligned} U_{\text{dispersion}} &= \underbrace{\frac{1}{2}\sum_{\mathbf{n},j,k} \frac{C_6^{jk}}{|\mathbf{r}_{jk}+\mathbf{n}|^6} - \frac{C_6^{jk,\text{recip}}[1-g(\beta|\mathbf{r}_{jk}+\mathbf{n}|)]}{|\mathbf{r}_{jk}+\mathbf{n}|^6}}_{\text{sum in direct space}} \\ &\quad + \underbrace{\frac{1}{2}\sum_{\mathbf{n},j,k} \frac{C_6^{jk,\text{recip}}[1-g(\beta|\mathbf{r}_{jk}+\mathbf{n}|)]}{|\mathbf{r}_{jk}+\mathbf{n}|^6}}_{\text{sum in reciprocal space}} \\ &= \frac{1}{2}\sum_{\mathbf{n},j,k} \frac{C_6^{jk}}{|\mathbf{r}_{jk}+\mathbf{n}|^6} \end{aligned} \tag{14}$$

The net effect of this direct-space modification is that the original potential, including exact LB combination rules, will be treated *exactly* all the way up to the cutoff, including the reciprocal-space contributions inside the cutoff. Outside the cutoff, the direct-space terms are no longer present; hence, the error there comes only from the slight combination rule modifications. Note that this should be compared to the extreme approximation of just using average density and parameters from the entire system with analytical dispersion corrections for the energy and completely ignoring the forces due to these interactions.

In order to account for the abrupt shift in the potential that happens at the cutoff, we also add the constant

$$\frac{-C_6^{jk} + C_6^{jk,\text{recip}}[1-g(\beta r_{\text{cutoff}})]}{r_{\text{cutoff}}^6} \tag{15}$$

to ensure that we maintain a continuous potential. This enables us to use geometric combination rules for the reciprocal calculations regardless of the combination rules in the applied force field, and as we will show in the following sections, this reduces the LB approximation error by an order of magnitude compared to that of our previous implementation.

3. METHODS

For the simulations of the palmitoyl-oleoyl-phosphocholine (POPC) bilayers in this work, we extended the simulations using LJ-PME with LB combination rules in our previous study.[22] The structures simulated originally came from the work of Hub et al.[29] and contain 128 POPC molecules and 5262 SPC[30] water molecules. The starting structure in the dimyristoyl-phosphocholine (DMPC) simulations was downloaded from the Stockholm Lipids[31−33] (Slipids) web page and

DOI: 10.1021/acs.jctc.5b00726
J. Chem. Theory Comput. 2015, 11, 5737−5746

contains 128 DMPC molecules and 3840 TIP3P[34] water molecules. The systems were first equilibrated for 50 ns and then simulated for an additional 500 ns at 298 K (POPC) or 323 K (DMPC) using a time step of 2 fs. Bond lengths were constrained using the LINCS[35] algorithm. Temperature was controlled with a Nosé−Hoover thermostat, and pressure was coupled semi-isotropically to 1 bar in the lateral and normal planes with the Berendsen[36] barostat during equilibration and the Parrinello−Rahman[37] barostat for production runs.

The POPC parameters were modified from the parameters of Berger[38] by using parameters for the double bond and atom types from the OPLS united atom force field.[39] For DMPC, the simulation utilized the parameters from the Slipids force field. Electrostatic interactions were evaluated every step using PME,[2] and the LJ interactions were evaluated by employing full exact LB combination rules, our previous approximation of geometric combination rules in reciprocal space, and finally the new direct-space corrections described in Section 2.2 together with geometric combination rules in reciprocal space. A fourth-order spline interpolation was applied for the PME calculations, together with a grid spacing of 1.2 Å. Finally, we also performed simulations using either a 10 Å (POPC) or 14 Å cutoff, together with dispersion corrections, for the LJ interactions. For all simulations, the real-space cutoff in the PME calculations was set to 10 Å both for Coulomb and LJ interactions.

For the performance benchmark simulations, we used three different systems: a box of SPC/E water,[40] a dipalmitoylphosphocholine (DPPC) bilayer, and a well-studied ion channel system containing the membrane protein GluCl.[41] The water system was constructed by placing 666 molecules in a cubic box and then condensing the system for 50 000 steps using a reference pressure of 10 bar and a temperature of 298 K. After this, the reference pressure was set to 1 bar, and the system was equilibrated for an additional 100 000 steps, reaching a final density of approximately 1 kg/L. For the production runs, this system was then replicated in three dimensions to reach the desired system size. The strong scaling simulations were carried out with a system size of 42 624 molecules, and the weak scaling was measured using systems with 42 624, 340 992, and 2 727 936 molecules and maintaining a load of roughly 250 particles per CPU core. The system was simulated using geometric combination rules and LJ-PME, and for the strong scaling, a reference simulation with an LJ cutoff of 10 Å and dispersion corrections was also performed. The simulations were performed using the Verlet cutoff scheme introduced in GROMACS-4.6, which also makes it possible to create GPU-accelerated implementations.[42]

The DPPC bilayer, containing 400 lipid molecules and 12 820 SPC/E waters, was constructed by replicating our previous DPPC system[22] along the x and y axes to make it 4 times larger. The system was first equilibrated using a conjugate gradient method using the tolerance 1 kJ mol^{-1} nm^{-1}, followed by an MD simulation using a time step of 0.2 fs for 30 000 steps, after which the time step was increased to 2 fs and an additional 30 000 steps were performed. Electrostatic interactions were evaluated using PME, LJ interactions by using a twin-range 10/16 Å cutoff updated every 10th step. DPPC parameters were taken from Chiu et al.[43] Benchmark simulations were carried out using a direct-space cutoff of 10 Å for both electrostatic and LJ-PME, and since the DPPC coefficients are derived using geometric combination rules, we treated both direct and reciprocal space in LJ-PME using these rules. Reference benchmarks were obtained from three simulations using different choices for the LJ setup: 10 Å cutoff, twin-range 10/14 Å or twin-range 10/16 Å, both with an update frequency of 10 steps, and dispersion corrections applied for all three setups. Other than the choice of treatment for the LJ interactions (and temperature), all of the DPPC systems were simulated using the same parameters as the POPC system above. The DPPC simulations were perfomed using the charge group cutoff scheme in GROMACS (later referenced as group scheme).

The ion channel system, consisting of GluCl embedded in a solvated bilayer (a total of 142 000 atoms), represents a typical membrane protein, which proved to be quite challenging to scale due to its relatively small size and inhomogeneous computational workload. The Amber99SB-ILDN force field[44] was used for the protein, and the lipids were modeled with the Berger force field parameters.[38] The benchmarks were set up with the GROMACS Verlet cutoff scheme, a time step of 2 fs, and H-bond constraints. To compare the performance of the GPU-accelerated LJ-PME implementation to the performance when treating LJ interactions with cutoffs, we carried out benchmarks with a 10 Å cutoff and geometric combination rules in reciprocal space for LJ-PME as well as runs with LJ interactions truncated at a slightly longer distance, 14 Å. The performance was measured over the second half of 3 min long runs, ensuring that the influence of initialization and initial load balancing on performance is small. Strong scaling is shown to 1100 atoms per node or 138 atoms per CPU core, which we believe is particularly impressive in combination with the very high absolute performance achieved on a single node.

All simulations were carried out with a modified development version of the GROMACS simulation package (based on version 5.0). The implementation of the modified direct-space interactions (Section 2.2) is part of the publicly available GROMACS-5.1, and the performance improvements will be included in future releases.

4. RESULTS

4.1. Modifying the Direct-Space Interactions Increases Accuracy. The implementation of the modified direct-space interactions (Section 2.2) in GROMACS was tested on the same POPC bilayer as that used in previous work[22] and an all-atom DMPC bilayer obtained from the Slipids webpage.[45] Simulations were performed with four different setups: (I) Full LB combination rules in both direct and reciprocal space, (II) approximation of reciprocal space with geometric combination rules, (III) modified direct-space interactions together with geometric combination rules in reciprocal space, and (IV) either a 10 Å (POPC) or 14 Å (DMPC) cutoff together with dispersion corrections.

From these simulations, the average area per lipid was calculated from the last 100 ns of simulation time, as reported in Table 1. In agreement with our previous results,[22] the area of 66.3 Å^2 obtained from simulation II of the POPC systems is very similar to the 67.5 Å^2 from simulation I, which supports the argument that the effects from the reciprocal-space approximation should be small for normal simulation properties. However, the addition of the direct-space modification present in simulation III reduces this difference even further with an area of 66.9 Å^2, which almost puts the values within the reported standard errors. The area of 71.4 Å^2 in simulation IV is far from these values and supports the notion that dispersion corrections are not sufficient to correctly account for the long-range interactions.

DOI: 10.1021/acs.jctc.5b00726
J. Chem. Theory Comput. 2015, 11, 5737−5746

Table 1. Calculated Areas Per Lipid from 500 ns Simulations of POPC or DMPC Using LJ-PME or Cutoffs for LJ Interactions[a]

	area/lipid [Å^2]			
	simulation I	simulation II	simulation III	simulation IV
POPC	67.5 ± 0.2	66.3 ± 0.2	66.9 ± 0.2	71.4 ± 0.1
DMPC	62.5 ± 0.2	64.3 ± 0.1	62.7 ± 0.2	62.8 ± 0.1

[a]Four different setups were utilized for the LJ interactions: (I) full treatment using LB combination rules, (II) approximation of reciprocal space using geometric combination rules, (III) geometric combination rules in reciprocal space combined with the modified interactions in direct space, or (IV) a 10 Å (POPC) or 14 Å (DMPC) cutoff. The averages are obtained from the last 100 ns of the simulations. The direct-space correction greatly improves the results when compared to the reference simulation (I).

In the DMPC system, there is a slight increase in the difference between simulations I (62.5 Å^2) and II (64.3 Å^2), but we also see a decrease in the difference compared to simulation III (62.7 Å^2), which puts simulations I and III within each other's standard errors. From simulation IV, we also see that the longer cutoff (14 Å) utilized in the Slipids force field enables the area per lipid to stay within standard errors of simulation I.

Furthermore, the high correlation between area per lipid at equilibrium and lipid chain ordering makes it possible to also study this effect through the deuterium order parameters. In Figures 1 and 2, we show the order parameters S_{cd} for both the

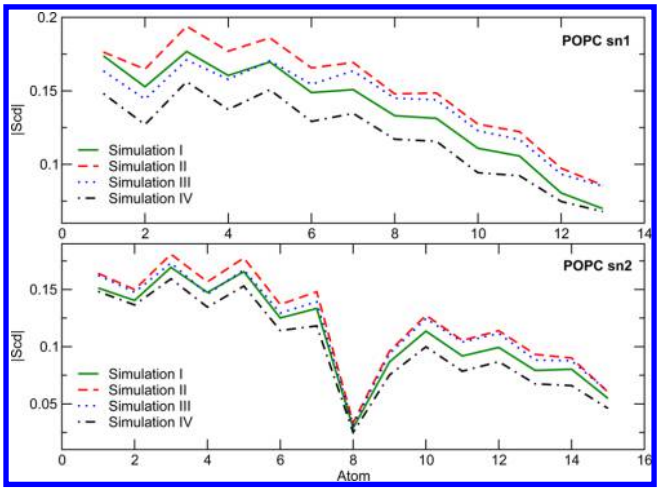

Figure 1. POPC deuterium order parameters averaged over the last 100 ns of simulation for the simulated systems. (I) Full treatment with LB combination rules, (II) approximation of reciprocal space using geometric combination rules, (III) geometric combination rules in reciprocal space and modified interactions in direct space, and (IV) 10 Å cutoff and dispersion correction.

sn1- and sn2-chains from simulations I–IV, calculated as an average over the last 100 ns of simulation using

$$S_{cd} = \frac{2}{3}S_{xx} + \frac{1}{3}S_{yy} \tag{16}$$

with S_{xx} and S_{yy} defined according to

$$S_{ij} = \frac{1}{2}\langle 3\cos\theta_i \cos\theta_j - \delta_{ij}\rangle \tag{17}$$

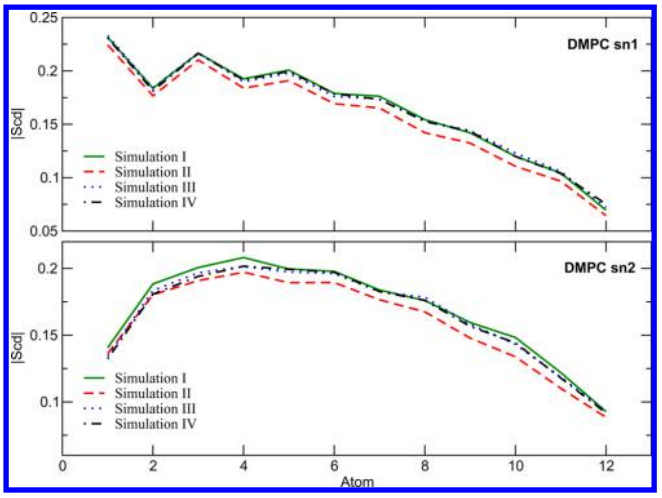

Figure 2. DMPC deuterium order parameters averaged over the last 100 ns of simulation for the simulated systems. (I) Full treatment with LB combination rules, (II) approximation of reciprocal space using geometric combination rules, (III) geometric combination rules in reciprocal space and modified interactions in direct space, and (IV) 14 Å cutoff and dispersion correction.

where θ_i represents the angle between the ith molecular axis and the bilayer normal.[46]

Starting with the calculated order parameters for POPC, the results for simulations II and IV from Table 1 are reinforced by the discrepancy in the order parameter of the sn1-chain compared to simulation I. The corrections introduced in simulation III bring the values very close to those of simulation I for the first carbon atoms in the chain, but the geometric approximation in the long-range part of the potential still seems to have a effect on the atoms past position six. For the sn2-chain, the existence of the double bond reduces the differences due to the conformational restrictions imposed on the atoms, but there is still a consistent trend in which simulation III is closer to the values obtained in simulation I compared to those for simulation II or IV.

For the DMPC simulations, the order parameters of simulations III and IV are almost identical to those of simulation I, with some small discrepancies at the beginning and at atom 10 of the sn2-chain. Simulation II follows the same pattern as that for POPC and has a small difference compared to simulation I, although the presence of hydrogens in the all-atom representation of the chains in DMPC seems to reduce this difference compared to the one obtained in the united-atom representation in the POPC simulation.

Furthermore, reorientational correlation functions were calculated for time differences of up to half of the last 100 ns of the total simulation time (Figures 3 and 4). The chosen vectors were either the P–N vector, connecting the phosphorus and nitrogen atoms in the lipid headgroup, or the C–C vector, connecting the first hydrophobic carbons (positioned directly after the carbonyl carbons) in each chain. The correlation functions were calculated using a first-order Legendre polynomial of the cosine of the angle.

For POPC (Figure 3), the correlation functions follow the same trend as the areas per lipid, with similar relaxation times for simulations I–III and a relatively large discrepancy displayed by simulation IV. The relaxation time for simulation III matches simulation I better than simulation II does, although the overall differences among the three simulations

DOI: 10.1021/acs.jctc.5b00726
J. Chem. Theory Comput. 2015, 11, 5737–5746

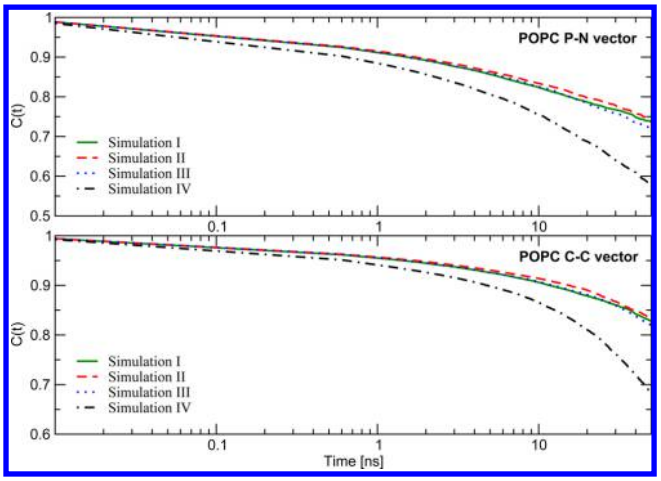

Figure 3. Rotational autocorrelation functions in POPC for the vector connecting the phosphorus and nitrogen atoms in the lipid headgroup (P−N) or the vector connecting the first hydrophobic carbons in each chain (C−C). (I) Full treatment with LB combination rules, (II) approximation of reciprocal space using geometric combination rules, (III) geometric combination rules in reciprocal space and modified interactions in direct space, and (IV) 10 Å cutoff and dispersion correction.

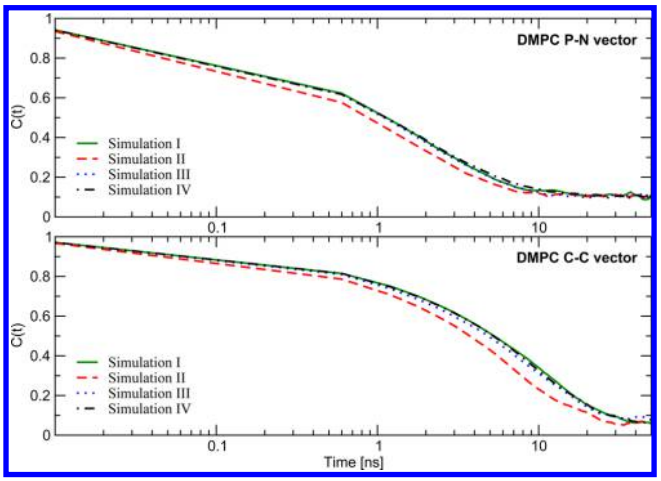

Figure 4. Rotational autocorrelation functions in DMPC for the vector connecting the phosphorus and nitrogen atoms in the lipid headgroup (P−N) or the vector connecting the first hydrophobic carbons in each chain (C−C). (I) Full treatment with LB combination rules, (II) approximation of reciprocal space using geometric combination rules, (III) geometric combination rules in reciprocal space and modified interactions in direct space, and (IV) 14 Å cutoff and dispersion correction.

are small. In the DMPC simulations (Figure 4), a fairly large discrepancy between the relaxation times in simulations I and II can be seen, whereas simulations III and IV seem to be almost identical to simulation I, with a small deviation seen in simulation III for the C−C vector.

The relative differences in the reorientational correlation functions were also present in the lateral diffusion coefficients of each lipid, as calculated from the last 100 ns of simulation. For POPC, the value in cutoff simulation IV (1.9×10^{-8} cm^2/s) was relatively far from the reference full LB value in simulation I (0.3×10^{-8} cm^2/s) when compared to that for simulation II or III (both at 0.8×10^{-8} cm^2/s). In the DMPC simulations, all values were much closer: 11.6 (I), 12.5 (II), 13.0 (III), and 12.6 (IV) $\times 10^{-8}$ cm^2/s. This might suggest that the entropic effects related to the double bond dynamics in POPC are more sensitive to the long-range treatment. Experimental diffusion coefficients of POPC[47−49] have been reported between 4 and 12.9 $\times 10^{-8}$ cm^2, which makes it difficult to draw definitive conclusions about absolute values (particularly given the small system sizes). However, it is evident that the results obtained using a cutoff of 10 Å deviate significantly from the more accurate treatment of LJ interactions. For DMPC, the experimental values[48,49] seem to be more stable around 12.5−12.6 $\times 10^{-8}$ cm^2, similar to what we obtain in our DMPC simulations, and the longer cutoff of 14 Å puts the simulation with truncated interactions closer to those using lattice summation.

Taken together, the structural data shows that it is important to accurately account for the effect from dispersive long-range interactions and that very small inaccuracies can lead to noticeable changes in the calculated properties. The previous implementation of LJ-PME, where the reciprocal-space interactions were approximated using geometrical combination rules, still achieves a reasonable accuracy with respect to the full lattice summation when comparing it to simulation IV in POPC, but the result is less satisfactory for DPMC. The introduction of the real-space correction presented here greatly reduces the remaining differences, which makes DMPC simulation III almost indistinguishable from simulation I for some properties and further improves the results for POPC. As a comparison, the simulations with a cutoff of 10 Å (previously the default setup) deviate significantly from simulation I, which supports the insufficiency of the dispersion correction to correctly account for the structural effects imposed by the long-range interactions. LJ cutoffs longer than 10 Å appear to be required in order to correctly account for all of the long-range interactions present in heterogeneous and anisotropic systems. From the DMPC simulation, it seems that a cutoff of 14 Å with dispersion corrections might get closer to the results of full lattice summation, but we would like to point out that for this system simulation III achieved an average performance that was 8% *higher* than the average performance of simulation IV. Thus, while a 14 Å cutoff might improve accuracy, LJ-PME provides both better performance and a more accurate summation. With the performance improvements discussed in Section 4.3, this difference will increase even further.

In addition to the structural analysis, we also performed a recalculation of all of the energies and forces at every frame in the trajectory from POPC simulation I using the other two LJ-PME methodologies to compare energies on identical structures, with results for the last 100 ns shown in Figure 5. The difference in total energy throughout the simulation when using only the approximation in reciprocal space (simulation II) gives an error of approximately 470−480 kJ/mol, or 0.1% of the total energy. When using the modified potential in direct space, the difference is reduced by an order of magnitude, to approximately 50 kJ/mol, thereby almost eliminating the statistical difference compared to the original simulation, which has an error estimate of 29 kJ/mol. The remaining difference might very well be due to the summation differences with single precision rather than the algorithm. This difference also holds true for the RMSD of the total force in the simulations. Here, the setup using parameters from simulation II results in a force RMSD of 0.168 kJ mol^{-1} nm^{-1}, whereas setup III achieves a force RMSD reduced to 0.0142 kJ mol^{-1} nm^{-1} (both compared to simulation I).

DOI: 10.1021/acs.jctc.5b00726
J. Chem. Theory Comput. 2015, 11, 5737−5746

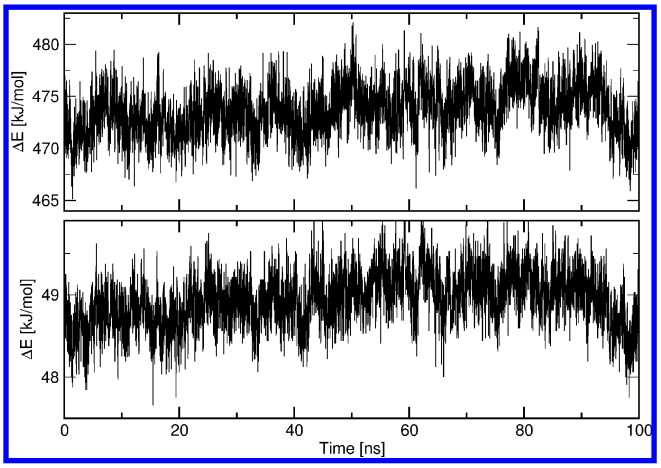

Figure 5. Absolute difference in total energy when re-evaluating interactions using reference coordinates. The top plot refers to simulation II settings with geometrical combination rules, and the bottom, simulation III settings that add the direct-space correction, both applied to the trajectory from simulation I. The difference in the energy is reduced by an order of magnitude in simulation III compared to that in simulation II. The total energy of the system is approximately −376 000 kJ/mol.

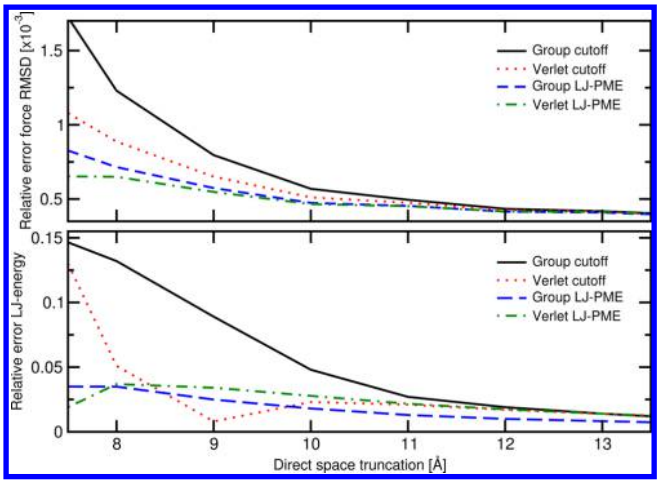

Figure 6. Force RMSD and relative differences in total Lennard-Jones energy calculated for the POPC system used in this work as a function of the truncation in direct space, using either LJ-PME or dispersion correction to correct for long-range LJ interactions. The reference systems utilized a direct-space cutoff of 20 Å, LJ-PME for long-range LJ interactions, and a reciprocal grid spacing of 0.2 Å with a sixth-order spline interpolation. Calculations were performed using either the Verlet[42] or group cutoff scheme in GROMACS.

4.2. Accuracy. To assess the accuracy improvements from the direct-space corrections and compare them to the other algorithms, a series of single-frame calculations was performed with different truncation schemes for the direct-space potentials (using the POPC bilayer from our previous work[22]). The reciprocal grid spacing was also modified with the same proportional change as the direct-space cutoff, starting at 1.2 Å for a cutoff of 10 Å. These calculations were compared to a reference setup in which we used a direct-space cutoff of 20 Å and a reciprocal grid with a spacing of 0.2 Å together with a sixth-order spline interpolation.

The LJ-PME calculations employed geometric combination rules and the direct-space correction introduced in this work, and we also performed the same calculations using a conventional cutoff together with dispersion correction for long-range LJ interactions. The calculations were performed using both the Verlet and group cutoff schemes available in GROMACS, and the results for these calculations can be seen in Figure 6.

For the cutoff calculations, there is a clear trend of the results getting more accurate as the cutoff is increased and the Verlet scheme displays a higher accuracy than the group scheme. When the cutoff goes below 10 Å, there is a large increase in the magnitude of the error, which indicates that the dispersion correction is inadequate in order to correctly account for the missing long-range effects. Although the error for the Verlet scheme goes down further as the cutoff is reduced from 10 to 9 Å, the shape of the curve suggests that this point is a statistical outlier, likely due to cancellation of errors.

In comparison, the errors in the LJ-PME calculations show very stable behavior as the cutoff is reduced below 10 Å, and increasing the cutoff beyond 10 Å does not seem to have a substantial effect on the overall accuracy. These comparably flat profiles of the error curves for LJ-PME suggest that it might be possible to decrease the real-space cutoff in simulations using LJ-PME without large reductions in the overall accuracy. There will, of course, be limitations to how far the cutoff can be reduced, which is indicated by the behavior of the errors for LJ-PME below 8 Å. These limitations have been discussed in the recent work by Isele-Holder et al.,[21] where it was noted that cutoffs shorter than twice the largest LJ diameter will most likely impact the system properties because effects from the truncation of the repulsion term start to become non-negligible. For the POPC system studied here, the LJ diameter of the methylene groups in the united-atom tails is approximately 4.1 Å, which suggests that results obtained with cutoffs lower than approximately 8.2 Å would be inaccurate to use.

From these calculations, we can see that LJ-PME maintains a high level of accuracy regardless of the applied cutoff in direct space. Furthermore, when comparing the errors with those from the cutoff simulations, we can see that the accuracy obtained with LJ-PME stays on par with what we achieve using a 10 Å cutoff and dispersion correction. This suggests that it should be possible to use LJ-PME with smaller direct-space cutoff than what the applied force field dictates. It also gives a good indication that future force fields, developed with dispersion solvers for all of the nonbonded interactions, hopefully can remove the cutoff restriction commonly imposed by force fields utilized today.

4.3. Performance. In our previous work,[22] we showed that the LJ-PME with LB combination reached only about 25% of the performance that GROMACS achieves with its cutoff setup. This is not surprising given the large amount of optimization (including GPU and SIMD code) that has gone into the nonbonded interactions in GROMACS, but in order for LJ-PME to be a realistic alternative, this is the absolute performance with which it must be competitive. By using geometric combination rules for the reciprocal part of the potential, the performance could be increased to almost 80% of the performance achieved when using a twin-range 10/16 Å cutoff. Here, we will show only numbers concerning geometric rules in reciprocal space since the newly implemented direct-space modification (Section 2.2) makes it unnecessary to use full reciprocal space LB combination rules in any normal simulation.

DOI: 10.1021/acs.jctc.5b00726
J. Chem. Theory Comput. 2015, 11, 5737−5746

The previously reported implementation of LJ-PME had challenges with scalability when the number of particles per core decreased to below 500, which was coupled with extremely prohibitive communication costs when performing all-to-all communication during the calculation of the three-dimensional FFTs. At the scaling limit, the number of messages, not their size, becomes the bottleneck. We have now implemented a combined all-to-all communication for the electrostatic and LJ-PME in order to reduce this cost by a factor of 2. Together with new analytical interaction kernels that also use SIMD (single-instruction, multiple-data) instructions (e.g., AVX on x86) for LJ-PME, this now enables LJ-PME to scale as well as the cutoff simulations in GROMACS, down to about 30 particles per core. The performance was measured on three separate systems: a box of SPC/E-water simulated at the Blue Gene/Q system at the Jülich Supercomputing Centre, a DPPC bilayer simulated on the Triolith supercomputer (Intel E5-2660 CPUs) at the National Supercomputer Centre in Linköping, and the ion channel system GluCl[41] simulated on the Piz Daint supercomputer (a hybrid Cray XC30 machine with Intel Xeon E5-2670 CPUs, NVIDIA Tesla K20X GPUs, and an Aries Dragonfly network) at the Swiss National Supercomputer Centre in Zürich.

On the Blue Gene/Q system, we investigated the weak and strong scaling limits of the LJ-PME implementation, and the results are displayed in Table 2. In the strong scaling simulations, LJ-PME maintains a relative performance of 70% compared to the one obtained using a single range 10 Å cutoff, a large improvement compared to the old implementation due to the fact that here we go all the way down to 32 atoms per core in the last simulation. We now observe similar performance characteristics for the cutoff and LJ-PME performance simulations, and the largest difference in absolute performance is coupled to the interpolation of the interaction coefficients onto the PME grid. In terms of absolute performance, when using 512 Blue Gene/Q cores and maintaining a 10 Å cutoff in direct space, this implementation uses only 6.4 ms per step, which can be compared to the only other LJ-PME implementation available (from the excellent work of Isele-Holder et al.[21]) that needs approximately 40 ms per step with a significantly shorter 7 Å cutoff when evaluating the interaction at every step on the same hardware setup.

Table 2. Strong and Weak Scalings Measured on a Blue Gene/Q System for a Simulation of SPC/E-Water[a]

strong scaling [ns/day]				
no. of cores	512	1024	2048	4096
LJ-PME	27	42	52	66
cutoff (10 Å)	37	58	76	92
weak scaling				
no. of cores		512	4096	32 768
performance [ns/day]		27	25	19
nonbonded forces [%]		45	43	33
PME mesh [%]		22	22	23

[a]The strong scaling was measured on a system of 42 624 water molecules, whereas the weak scaling was measured using 250 particles per core. The absolute performance is presented in ns/day, and for the weak scaling, the time spent calculating the PME mesh or direct-space nonbonded interactions is shown relative to the total simulation time.

In regard to weak scaling, LJ-PME performs only slightly worse than linear when going from 512 to 4096 cores. The small performance loss is coupled with the increased communication costs in the domain decomposition, neighbor search, and coordinate communication. Increasing the number of cores by an additional factor of 8 incurs a slightly larger degradation in performance, which is coupled with an increase in the cost of the redistribution of particle positions and forces within the PME ranks, along with the interpolation of the interaction coefficients onto the PME grid. Since these regions were found to be the limiting factor in the measurements of both strong and weak scalings, they are now under consideration for future improvements to the algorithm.

From the DPPC simulations (Figure 7), we see that when simulating a more heterogeneous system the current implementation has an absolute performance that is slightly *faster* than a cutoff simulation using a twin-range 10/16 Å cutoff, and it stays at around 90−100% of what is achieved with the 10/14 Å cutoff (16 cores being an outlier with a relative performance of approximately 80%). Compared to the simulations with a cutoff of 10 Å, LJ-PME still performs well, with a relative performance of approximately 75−80% (85% at 512 cores as the highest, and 72% at 16 cores the lowest), which can be compared to 10/14 Å, which stays at a relative performance of 80−90% (compared to 10 Å) and 10/16 Å at 70−80%. It is worth pointing out that these differences are smaller than the relative hit incurred from first enabling electrostatics PME, and they are measured relative to very highly tuned cutoff kernels.

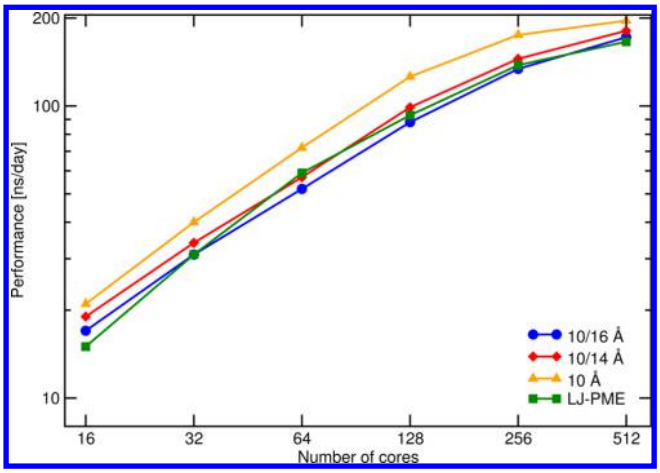

Figure 7. Performance for DPPC bilayer simulations (58 460 atoms in total) treating LJ interactions with either cutoffs (10 Å or twin-range 10/14 Å and 10/16 Å) or using LJ-PME with geometric combination rules in reciprocal space. The simulations were performed on Intel E5-2660 CPUs, and performance was measured over 50 000 simulation steps.

In order to assess the performance obtained with LJ-PME on more complex systems commonly simulated, we also performed benchmarks on the well-studied ion channel GluCl, with results in Figure 8. On heterogeneous hardware, such as the setup on Piz Daint, GROMACS offloads nonbonded interactions to GPUs and therefore the performance is very sensitive to the CPU-GPU balance. The Cray XC30 hybrid machine represents a well-balanced setup where the GPUs are fast enough to reduce the cost of computing short-range nonbonded interactions to the point where it is possible to use cutoffs that are longer than default, up to 12−14 Å, without any additional loss of performance. Because of this,

DOI: 10.1021/acs.jctc.5b00726
J. Chem. Theory Comput. 2015, 11, 5737−5746

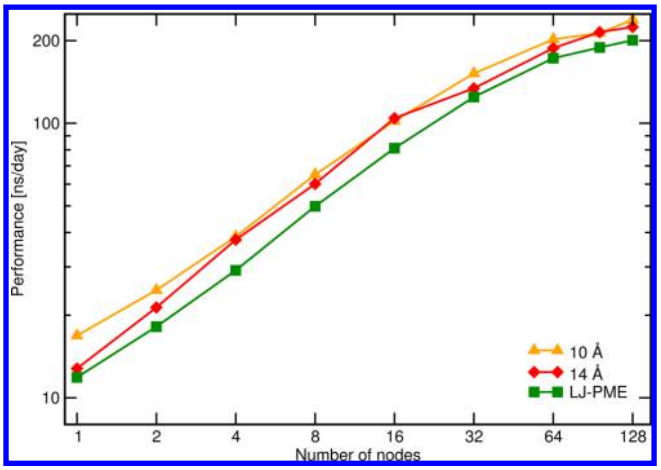

Figure 8. Performance for GluCl membrane protein simulation (142 000 atoms) with LJ interactions treated using either a 10 or 14 Å cutoff or with LJ-PME using geometric combination rules and direct-space corrections. The simulations were performed on a heterogeneous hardware setup, with each node containing Intel Xeon E5-2670 CPUs and an NVIDIA Tesla K20X GPU. Performance was measured over the second half of 3 min runs.

the overall performance, as shown in Figure 8, is bound by the PME performance from around 4 nodes and above. This has the effect of making the difference between the simulations using cutoffs almost negligible and hence making the comparison with the LJ-PME implementation even more challenging. Still, on a single node, the GPU-accelerated LJ-PME implementation manages to achieve 70 and 92% of the performance of the simulations utilizing 10 and 14 Å cutoffs, respectively. It also exhibits strong scaling similar to the cutoff simulations, achieving 81 and 96% of the 10 and 14 Å cutoff simulations on 128 XC30 nodes, respectively. The CUDA LJ-PME nonbonded kernels using geometric combination rules are only about 20% slower than the LJ cutoff kernels; therefore, on other hybrid machines with relatively less GPU computational power, LJ-PME will have an even greater advantage compared to the use of longer cutoffs.

5. CONCLUSIONS

This work proposes a new correction for LJ-PME that is applied in direct space, which makes it possible to use geometrical combination rules in reciprocal space and yet maintain full LB combination rules for all interactions out to the cutoff. This preserves an exact description of both potential and force up to the cutoff, and there is only a very small remaining approximation (a factor 10 lower than before) outside the cutoff. This should be compared to analytical dispersion corrections, where all forces outside the cutoff are ignored and the potential is calculated based on average density and parameters. This combines the accuracy of LB combination rules with the huge computational advantage of using geometric combination rules in reciprocal space. Furthermore, we have made optimizations to the communication bottlenecks, and together with new accelerated nonbonded kernels for the direct-space interactions in LJ-PME, we now attain a performance that is very close to standard cutoff simulations in GROMACS and, to the best of our knowledge, that is significantly faster than any other available implementation. This should finally help to lay aside the issue of performance degradation from mesh-based dispersion solvers. With the first implementations of electrostatic PME, we were looking at a performance degration far worse than this, and with the possible implementation of a multiple time step algorithm in a future version of GROMACS, there is even potential to improve performance beyond what is possible with cutoffs in GROMACS.

LJ-PME now enables the correct treatment of long-range LJ interactions in simulations of inhomogeneous systems, which, until recently, have been treated with artificial cutoffs and insufficient long-range corrections that assume isotropic surroundings. For electrostatic interactions, the severe effects coupled to the use of cutoffs[7] were quickly understood by the community, but for dispersion interactions, the issue seems to be more subtle. The inclusion of long-range dispersion effects has been shown to have non-negligible effects on structural properties such as area per lipid and surface tension,[14,22,50−52] and we have previously shown that LJ-PME can be used with existing force fields. Recently, our new GROMACS LJ-PME implementation has also been shown to improve the accuracy of free energy calculations.[53] While current force fields have been parametrized using analytical dispersion corrections, this is not as severe of a limitation as it might first seem since parameters are typically derived from extremely simple systems where the assumptions of homogeneity and isotropy are a quite good approximation. There might still be room to improve parameters further by using LJ-PME, but even with current force fields, it is likely to be a significant improvement.

The use of mesh-based solvers for all long-range interactions transforms the cutoff into a possible tuning parameter.[21] Therefore, correct treatment of all long-range interactions would remove the cutoff restriction present in existing force fields and provide an accurate force field where the cutoff is used as an extra tuning parameter to achieve the highest performance.

AUTHOR INFORMATION

Corresponding Author

*E-mail: erik.lindahl@scilifelab.se.

Funding

This work was supported by grants from the Swedish Foundation for Strategic Research, the Swedish Research Council (2010-491, 2010-5107), the CRESTA EU FP7 project (287703), the European Research Council (258980), and the Swedish e-Science Research Center. Computer resources on the Triolith supercomputer were provided through the Swedish National Infrastructure for Computing (SNIC 020/11-41).

Notes

The authors declare no competing financial interest.

ACKNOWLEDGMENTS

We would like to acknowledge the Jülich Supercomputing Center (JSC) for BlueGene/Q computing resources and the Swiss National Supercomputing Centre (CSCS, project ID g43) for the Piz Daint computing resources.

REFERENCES

(1) Darden, T.; York, D.; Pedersen, L. *J. Chem. Phys.* **1993**, *98*, 10089−10092.
(2) Essmann, U.; Perera, L.; Berkowitz, M. L.; Darden, T.; Lee, H.; Pedersen, L. G. *J. Chem. Phys.* **1995**, *103*, 8577−8592.
(3) Hess, B. *J. Chem. Phys.* **2002**, *116*, 209−217.
(4) Hünenberger, P. H.; van Gunsteren, W. F. *J. Chem. Phys.* **1998**, *108*, 6117−6134.

DOI: 10.1021/acs.jctc.5b00726
J. Chem. Theory Comput. 2015, 11, 5737−5746

(5) Mark, P.; Nilsson, L. *J. Comput. Chem.* **2002**, *23*, 1211−1219.
(6) Anézo, C.; de Vries, A. H.; Höltje, H.-D.; Tieleman, D. P.; Marrink, S.-J. *J. Phys. Chem. B* **2003**, *107*, 9424−9433.
(7) Patra, M.; Karttunen, M.; Hyvonen, M. T.; Falck, E.; Lindqvist, P.; Vattulainen, I. *Biophys. J.* **2003**, *84*, 3636−3645.
(8) Feller, S. E.; Pastor, R. W.; Rojnuckarin, A.; Bogusz, S.; Brooks, B. R. *J. Phys. Chem.* **1996**, *100*, 17011−17020.
(9) Lindahl, E.; Hess, B. A.; van der Spoel, D. *J. Mol. Mod.* **2001**, *7*, 306−317.
(10) Lagüe, P.; Pastor, R. W.; Brooks, B. R. *J. Phys. Chem. B* **2004**, *108*, 363−368.
(11) Wu, X.; Brooks, B. R. *J. Chem. Phys.* **2005**, *122*, 044107.
(12) Wu, X.; Brooks, B. R. *J. Chem. Phys.* **2008**, *129*, 154115.
(13) Klauda, J. B.; Wu, X.; Pastor, R. W.; Brooks, B. R. *J. Phys. Chem. B* **2007**, *111*, 4393−4400.
(14) Venable, R. M.; Chen, L. E.; Pastor, R. W. *J. Phys. Chem. B* **2009**, *113*, 5855−5862.
(15) in't Veld, P. J.; Ismail, A. E.; Grest, G. S. *J. Chem. Phys.* **2007**, *127*, 144711.
(16) Tameling, D.; Springer, P.; Bientinesi, P.; Ismail, A. E. *J. Chem. Phys.* **2014**, *140*, 024105.
(17) Shirts, M. R.; Mobley, D. L.; Chodera, J. D.; Pande, V. S. *J. Phys. Chem. B* **2007**, *111*, 13052−13063.
(18) Hockney, R. W.; Eastwood, J. W. *Computer Simulation Using Particles*; McGraw-Hill: New York, 1981.
(19) Plimpton, S. *J. Comput. Phys.* **1995**, *117*, 1−19.
(20) Isele-Holder, R. E.; Mitchell, W.; Ismail, A. E. *J. Chem. Phys.* **2012**, *137*, 174107.
(21) Isele-Holder, R. E.; Mitchell, W.; Hammond, J. R.; Kohlmeyer, A.; Ismail, A. E. *J. Chem. Theory Comput.* **2013**, *9*, 5412−5420.
(22) Wennberg, C. L.; Murtola, T.; Hess, B.; Lindahl, E. *J. Chem. Theory Comput.* **2013**, *9*, 3527−3537.
(23) Good, R. J.; Hope, C. J. *J. Chem. Phys.* **1971**, *55*, 111−115.
(24) Lorentz, H. A. *Ann. Phys.* **1881**, *248*, 127−136.
(25) Ewald, P. P. *Ann. Phys.* **1921**, *369*, 253−287.
(26) Karasawa, N.; Goddard, W. A., III *J. Phys. Chem.* **1989**, *93*, 7320−7327.
(27) Toukmaji, A.; Board, J. A. *Comput. Phys. Commun.* **1996**, *95*, 73−92.
(28) Deserno, M.; Holm, C. *J. Chem. Phys.* **1998**, *109*, 7678−7693.
(29) Hub, J. S.; Winkler, F. K.; Merrick, M.; de Groot, B. L. *J. Am. Chem. Soc.* **2010**, *132*, 13251−13263.
(30) Berendsen, H. J. C.; Postma, J. P. M.; van Gunsteren, W. F.; Hermans, J. In *Intermolecular Forces*; Pullman, B., Ed.; D. Reidel Publishing Company: Dordrecht, The Netherlands, 1981; pp 331−342.
(31) Jämbeck, J. P. M.; Lyubartsev, A. P. *J. Phys. Chem. B* **2012**, *116*, 3164−3179.
(32) Jämbeck, J. P. M.; Lyubartsev, A. P. *J. Chem. Theory Comput.* **2012**, *8*, 2938−2948.
(33) Jämbeck, J. P. M.; Lyubartsev, A. P. *J. Chem. Theory Comput.* **2013**, *9*, 774−784.
(34) Jorgensen, W. L.; Chandrasekhar, J.; Madura, J. D.; Impey, R. W.; Klein, M. L. *J. Chem. Phys.* **1983**, *79*, 926−935.
(35) Hess, B. *J. Chem. Theory Comput.* **2008**, *4*, 116−122.
(36) Berendsen, H. J. C.; Postma, J. P. M.; van Gunsteren, W. F.; DiNola, A.; Haak, J. R. *J. Chem. Phys.* **1984**, *81*, 3684−3690.
(37) Parrinello, M.; Rahman, A. *J. Appl. Phys.* **1981**, *52*, 7182−7190.
(38) Berger, O.; Edholm, O.; Jähnig, F. *Biophys. J.* **1997**, *72*, 2002−2013.
(39) Jorgensen, W. L.; Tirado-Rives, J. *J. Am. Chem. Soc.* **1988**, *110*, 1657−1666.
(40) Berendsen, H. J. C.; Grigera, J. R.; Straatsma, T. P. *J. Phys. Chem.* **1987**, *91*, 6269−6271.
(41) Yoluk, O.; Brömstrup, T.; Bertaccini, E.; Trudell, J.; Lindahl, E. *Biophys. J.* **2013**, *105*, 640−647.
(42) Páll, S.; Hess, B. *Comput. Phys. Commun.* **2013**, *184*, 2641−2650.
(43) Chiu, S.; Pandit, S. A.; Scott, H. L.; Jakobsson, E. *J. Phys. Chem. B* **2009**, *113*, 2748−2763.
(44) Lindorff-Larsen, K.; Piana, S.; Palmo, K.; Maragakis, P.; Klepeis, J. L.; Dror, R. O.; Shaw, D. E. *Proteins: Struct., Funct., Genet.* **2010**, *78*, 1950−1958.
(45) Stockholm Lipids. http://mmkluster.fos.su.se/slipids/.
(46) Egberts, E.; Marrink, S. J.; Berendsen, H. J. C. *Eur. Biophys. J.* **1994**, *22*, 423−436.
(47) Ladha, S.; Mackie, A. R.; Harvey, L. J.; Clark, D. C.; Lea, E. J. A.; Brullemans, M.; Duclohier, H. *Biophys. J.* **1996**, *71*, 1364−1373.
(48) Filippov, A.; Orädd, G.; Lindblom, G. *Biophys. J.* **2003**, *84*, 3079−3086.
(49) Vaz, W. L. C.; Clegg, R. M.; Hallmann, D. *Biochemistry* **1985**, *24*, 781−786.
(50) Klauda, J. B.; Venable, R. M.; Freites, J. A.; O'Connor, J. W.; Tobias, D. J.; Mondragon-Ramirez, C.; Vorobyov, I.; MacKerell, A. D.; Pastor, R. W. *J. Phys. Chem. B* **2010**, *114*, 7830−7843.
(51) Janeček, J. *J. Phys. Chem. B* **2006**, *110*, 6264−6269.
(52) Shi, B.; Sinha, S.; Dhir, V. K. *J. Chem. Phys.* **2006**, *124*, 204715.
(53) Fischer, N. M.; van Maaren, P. J.; Ditz, J. C.; Yildirim, A.; van der Spoel, D. *J. Chem. Theory Comput.* **2015**, *11*, 2938−2944.

DOI: 10.1021/acs.jctc.5b00726
J. Chem. Theory Comput. 2015, 11, 5737−5746